

# Microstructural effect on oxidation kinetics of NbSi<sub>2</sub> at 1023 K

F. Zhang, L.T. Zhang\*, A.D. Shan, J.S. Wu

Key Laboratory of the Ministry of Education for High Temperature Materials and Testing, School of Materials Science and Engineering, Shanghai Jiao Tong University, Shanghai 200030, PR China

Received 4 November 2005; accepted 7 December 2005

Available online 24 January 2006

## Abstract

Poly- and single crystalline NbSi<sub>2</sub> specimens with different microstructures were prepared by arc-melting, spark plasma sintering (SPS) and optical-heating floating zone melting for oxidation experiments at 1023 K. The effects of cracks, pores and grain boundary in the microstructure on the oxidation behavior of NbSi<sub>2</sub> were investigated. For arc-melted poly-crystalline specimens containing micro-cracks, NbSi<sub>2</sub> fully turned into powders after 3 h exposure at 1023 K, which is known as the “pestring” phenomenon. As a comparison, no pestring was found in the dense SPS poly-crystalline specimens and single crystals after 89 h. The oxide scale consists of Nb<sub>2</sub>O<sub>5</sub> and SiO<sub>2</sub>. The oxidation kinetics of all specimens follows a linear law. The oxidation rate was higher in the poly-crystalline specimen in comparison to single crystalline. The mechanism of oxidation has been analysed using a kinetic model.

© 2005 Elsevier B.V. All rights reserved.

**Keywords:** Intermetallics; Crystal growth; Grain boundary; Oxidation

## 1. Introduction

Refractory transition-metal disilicides such as MoSi<sub>2</sub> and NbSi<sub>2</sub> are promising materials for high temperature structural applications because of their low density, high melting points and high strength [1–4]. However, the application of Nb–Si alloys is limited because of their poor oxidation resistance at high temperatures. Especially, pestring oxidation of NbSi<sub>2</sub> occurs at 1023 K after a certain period of exposure in air. Pestring oxidation in NbSi<sub>2</sub> was first reported by Rausch [5] and was further confirmed by Pitman and Tsakirooulos [6] and Murakami et al. [7]. Al, B and Cr additions are found to improve the oxidation resistance of NbSi<sub>2</sub> at 1523 K [8,9]. However, the Al-doped NbSi<sub>2</sub> still displayed pestring at 1023 K. Since most of the attention for pestring phenomenon has been paid to MoSi<sub>2</sub>, the study of NbSi<sub>2</sub> is relatively scarce.

According to many observations in MoSi<sub>2</sub>, it is found that defects such as cracks, pores and grain boundary in microstructure are related to pestring. Although early works attributed the pestring to high residual stresses accumulated during cooling

from melt [10–12]. It is not very likely for brittle materials such as MoSi<sub>2</sub> and NbSi<sub>2</sub> due to the fact that the thermal stress may well be released by forming a number of micro-cracks in the matrix. In an arc-melted ingot, many cracks are usually seen in the microstructure of these compounds. Later works [13] noticed the effects from structural defects and imperfections such as pores and cracks in the bulk material on the catastrophic fragmentation. Bertiss et al. [14] studied the oxidation behavior of MoSi<sub>2</sub> prepared by different processes and found that the oxidation behaviors were a function of microstructure. Only those materials containing micro-cracks in the microstructure experienced fragmentation during oxidation at 773 K. Kurokawa et al. [15] compared low temperature oxidation of fully dense and porous MoSi<sub>2</sub> and found accelerated oxidation and pestring in porous material only. It is proposed that volume expansion of oxide formed at cracks results in a wedging effect [16]. In contrast, Chou and Nieh [17] found that both as-cast and dense poly-crystalline MoSi<sub>2</sub> underwent severe pestring and MoSi<sub>2</sub> single crystal also disintegrated into small pieces when oxidized at 773 K. Whether there is similarity in pestring behavior between NbSi<sub>2</sub> and MoSi<sub>2</sub> forms a motivation of the present work.

In this paper, we first compare different pestring behaviors of as-cast, spark plasma sintered poly-crystalline NbSi<sub>2</sub> and NbSi<sub>2</sub> single crystal at 1023 K. Effects of cracks, pores and

\* Corresponding author at: School of Materials Science and Engineering, Shanghai Jiao Tong University, 1954 Hua Shan Road, Shanghai 200030, PR China. Tel.: +86 21 6293 2566; fax: +86 21 5254 0011.

E-mail address: lantingzh@sjtu.edu.cn (L.T. Zhang).

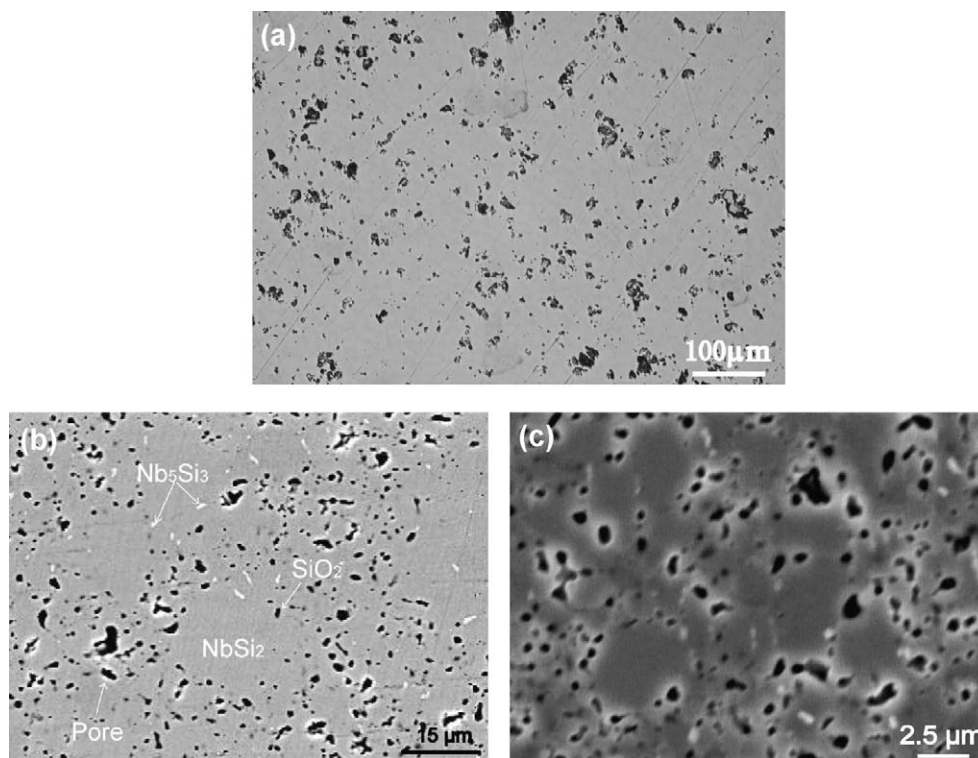


Fig. 1. Scanning electron images of NbSi<sub>2</sub> prepared by different processes: (a) arc-melted; (b) sintered by SPS at 30 MPa (back-scattered electron image); (c) sintered at 60 MPa (hot corrosion image).

grain boundary on oxidation behavior have been investigated focusing on the oxidation kinetics. A model has been proposed to describe the observed oxidation kinetics.

## 2. Experimental procedure

Poly-crystalline specimens were prepared by arc-melting and spark plasma sintering (SPS). Stoichiometric amounts of high purity elements (Nb, Si) were mixed and melted together in an arc-melting furnace on a water-cooled plate under purified Ar atmosphere to prepare poly-crystalline ingots. The arc-melted ingots were crushed into powder and ball-milled. The powder was sieved (below 30 μm in diameter) and loaded in a graphite crucible for sintering. The sintering was performed at 1573 K under a load between 30 and 60 MPa. Single crystal was grown by the optical-heating floating zone method on Asgal FZ-20035WHV apparatus. The crystal was grown from bottom to top in a vertical direction applying a growth rate in the range of 5–10 mm/h.

Oxidation behaviors of the specimens were characterized by measuring their oxidation kinetics at 1023 K in room air. Specimens approximately 5 mm × 5 mm × 1 mm in dimension were cut from the as-cast ingot, sintered bulk and as-grown single crystals (perpendicular to growth direction). The specimens were polished to mirror finish and cleaned in acetone and alcohol consequently prior to observation. Microstructures of the specimens prepared by different methods were examined using scanning electron microscope (SEM) and electron probe micro-analyser (EMPA). The orientation of single crystals was determined by Laue back-reflection method. Average grain size of the sintered poly-crystal NbSi<sub>2</sub> was determined by observing the fractural surface or by hot corrosion method. For those specimens fractured in a transgranular way, the grains were clearly seen in the fractured surface. Other specimens were first polished and oxidized to reveal their grains. Density of single and poly-crystalline NbSi<sub>2</sub> was measured by the Archimedes method. After oxidation, the phase constitutions of oxide products were characterized by X-ray diffraction (Cu Kα). X-ray photoelectron spectroscopy (XPS) was applied to analyze the elemental composition and chemical environments of Nb, Si and O elements in the oxide scale.

## 3. Results

### 3.1. Microstructure

The arc-melted poly-crystalline NbSi<sub>2</sub> contains quite a number of pre-existing microcracks and pores (Fig. 1(a)). This may be caused by the residual thermal stress on cooling during arc-melting. Microstructure analysis showed that the arc-melted ingot was of monolithic NbSi<sub>2</sub> phase. Laue diffraction confirmed transformation from poly-crystalline to single crystalline NbSi<sub>2</sub> after the zone melting, whose growth plane was close to (within 5°) (1 1  $\bar{2}$  0). Typical microstructures of the sintered NbSi<sub>2</sub> prepared under different conditions are shown in Fig. 1(b) and (c). Compared to the arc-melted ingot, a main feature of the microstructure is that it contains a few pores but not cracks. A relative density of more than 90% can be obtained by SPS. The relative density increased from 93.8 to 95% when the pressure during sintering increased from 30 to 60 MPa. Besides many pores, some minor phases such as Nb<sub>5</sub>Si<sub>3</sub> (bright particle in Fig. 1(b) and SiO<sub>2</sub> (dark phase in Fig. 1(b)) can be seen in the NbSi<sub>2</sub> matrix which is mainly due to the oxidation and volatilization of silicon during sintering. Similar microstructure was also reported for sintered MoSi<sub>2</sub> [18–20]. Average sizes of the two NbSi<sub>2</sub> specimens were determined to be 2.5 μm (30 MPa) and 3.9 μm (60 MPa), respectively.

### 3.2. Oxidation behavior

The oxidation kinetics curves of different NbSi<sub>2</sub> specimens are plotted in Fig. 2, showing the mass change versus time at

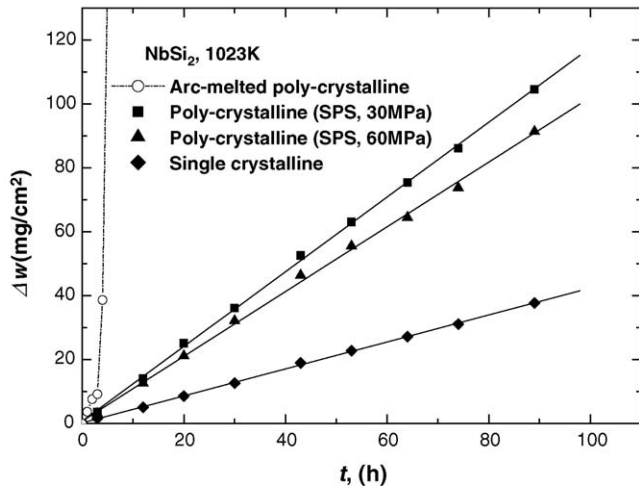


Fig. 2. Weight change as a function of exposure time for poly- and single crystalline NbSi<sub>2</sub> at 1023 K.

1023 K in air. Arc-melted specimen with many micro-cracks exhibited relatively rapid weight gain and fully turned into powder after 3 h exposure in air, which is known as pesting. However, for the dense sintered poly-crystalline specimens and single crystal, no fragmentation was found at a much longer exposure time, indicating that the pre-existing cracks are crucial to pest oxidation. Our previous in situ observation of NbSi<sub>2</sub> clearly shows that new cracks initiate from the pre-existing cracking sites [21]. Since the oxide spall from the matrix during the oxidation, the oxidation kinetics of NbSi<sub>2</sub> almost follows a linear law showing no indication of accelerated oxidation within the time period of observation. As shown in Fig. 2, the NbSi<sub>2</sub> poly-crystalline specimens show a much larger weight change than that of the single crystalline specimen, and the poly-crystalline specimen sintered at 30 MPa shows a higher weight change than one sintered at 60 MPa. This indicates that grain boundary and pores may probably accelerate the rate of oxidation reaction and will be modeled in the discussion part.

### 3.3. Phase constitution of the oxidation product

Fig. 3 shows XRD profiles of the oxide formed on poly- and single crystalline NbSi<sub>2</sub> after exposure at 1023 K for 89 h. There is no qualitative difference in the profiles between the poly-crystal (SPS) and single crystal materials, indicating that phase constitutions of the oxides formed on the two materials are almost the same. According to the XRD profiles, the oxide is identified to be mainly Nb<sub>2</sub>O<sub>5</sub> and a small amount of SiO<sub>2</sub>. XPS further determined Nb 3d and Si 2p states in the oxide scale (Fig. 4). According to Ref. [22], the peaks in Fig. 4(a) can be assigned as Nb<sup>5+</sup>. No other states of the elements were identified. Since only three elements Nb, Si and O were identified in the XPS spectra, the Nb and Si are probably in the form of oxide, as shown in the XRD profiles. Since the crystalline SiO<sub>2</sub> peaks are weak in the XRD profiles, most of the silica formed at 1023 K is probably in the amorphous form. This result is consistent with other alloys and compounds in the Nb–Si system [23].

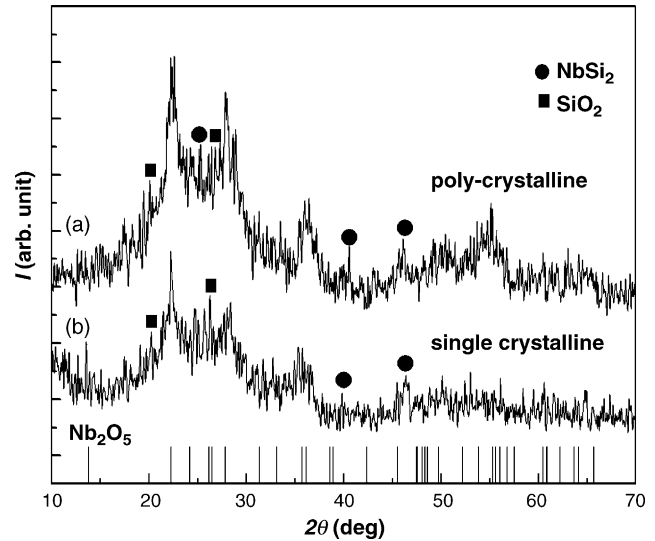


Fig. 3. XRD profiles of the oxide formed on NbSi<sub>2</sub> after exposure at 1023 K for 89 h in air for: (a) poly-crystalline specimen; (b) single crystalline specimen. The bars at the bottom of the plotting indicate peak positions of Nb<sub>2</sub>O<sub>5</sub> from JCPDS card no. 22-1196.

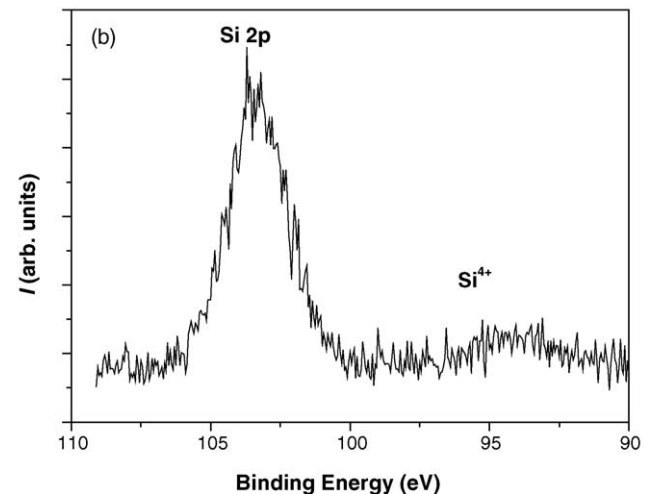
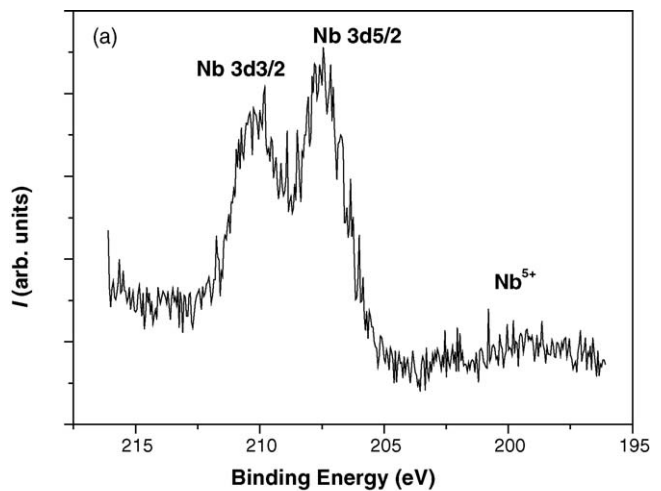


Fig. 4. XPS spectra showing the (a) Nb 3d and (b) Si 2p peaks of the oxide scale formed on NbSi<sub>2</sub> after exposure at 1023 K for 89 h.

Table 1  
Microstructural and oxidation kinetics parameters of single and poly-crystalline NbSi<sub>2</sub>

Specimen	Relative density ( $\rho/\rho_{\text{NbSi}_2}^{\text{th}}$ ) (%)	Average grain size ( $\mu\text{m}$ )	Linear oxidation rate constant $K_1$ (mg/cm <sup>2</sup> h) in Eq. (1)	Relative area during oxidation <sup>a</sup>
Single crystal	100	–	0.4	1
Poly-crystal (SPS@30 MPa)	93.8	2.5	1.2	2.8
Poly-crystal (SPS@60 MPa)	95.0	3.9	1.0	2.1

<sup>a</sup> Calculated from  $S'/S$  according to Eq. (3).

#### 4. Discussion

In general, the oxidation kinetics of a material can be described by the following equation:

$$\left(\frac{\Delta m}{S}\right)^n = Kt \quad (1)$$

where  $\Delta m$  is the mass change,  $S$  the surface area of a specimen,  $t$  the exposure time,  $K$  the rate constant of oxidation, and  $n$  is the exponent number ( $n = 1$ , linear law;  $n = 2$ , parabolic rate law;  $n = 3$ , cubic law) [24]. Fitting the data in Fig. 2 to Eq. (1) shows that the oxidation of NbSi<sub>2</sub> at 1023 K follows a linear law with the rate constant  $K$  being 0.4, 1.0 and 1.2 mg/cm<sup>2</sup> h for single crystal, dense and porous poly crystal, respectively. This indicates that the oxide formed on NbSi<sub>2</sub> is non-protective. XRD and XPS indicate the oxidation product to be Nb<sub>2</sub>O<sub>5</sub> and SiO<sub>2</sub>, thus the oxidation of NbSi<sub>2</sub> at 1023 K can be described as the following reaction:



The loose Nb<sub>2</sub>O<sub>5</sub> spalls from the specimen and prevents formation of a continuous scale of SiO<sub>2</sub> (crystalline and amorphous) on the NbSi<sub>2</sub> matrix during oxidation. Therefore, the oxidation of NbSi<sub>2</sub> is a simultaneous reaction of oxygen with freshly exposed matrix and the reaction rate is intrinsically determined by the reaction at matrix/gas interface.

Table 1 summarizes the average grain size, density and linear rate constant of three dense NbSi<sub>2</sub> specimens, which clearly indicates that grain boundary and porosity contribute to an increased oxidation rate. The non-protective nature of Nb<sub>2</sub>O<sub>5</sub> determines that there is no rate limiting process during the oxidation of NbSi<sub>2</sub> at 1023 K, whose reaction rate is merely controlled by the effective free surface exposed to gas atmosphere. For a fully dense single crystal without any grain boundary, the effective

free surface is equal to its nominal free surface area (Fig. 5(a)). However, for the poly-crystalline specimens containing grain boundaries and pores which are the quick diffusion paths for oxygen atoms, the effect from the grain boundary and pore can be considered to a direct increase to be the effective free surface of the material (Fig. 5(b)). Supposing oxygen atom (ion) penetrates at a certain depth  $h$  into the matrix (Fig. 5(b)), the effective reaction area  $S'$  can be estimated as follows:

$$S' = \left(\frac{S}{(\pi/4)L^2}\pi Lh + S\right) \frac{1}{\mu} = \frac{S}{\mu} \frac{4h + L}{L} \quad (3)$$

where  $S$  is the apparent surface area;  $L$  the mean grain size;  $\mu$  is the relative density of the specimen. ( $S/((\pi/4)L^2)$ ) estimates the number of grains within the region of interest; and the length of grain boundary is estimated as ( $S/((\pi/4)L^2)$ ) $\pi L$ . Thus the increased surface area due to grain boundary at a penetration depth  $h$  can be estimated as:

$$\frac{S}{(\pi/4)L^2}\pi Lh$$

According to a previous investigation on the cross-sectional microstructure of the oxide scale formed on NbSi<sub>2</sub>, the penetration depth of oxygen into the matrix is on the order of 1  $\mu\text{m}$  at 1023 K [6]. The calculated ratios of ( $S'/S$ ) in Eq. (3) are 2.8 and 2.1, respectively for the two sintered poly-crystalline specimens (Table 1), which coincide well with the relative ratio of the fitted oxidation rate constants of the three specimens. This clearly shows that the oxidation rate is determined by the effective exposure area.

Due to the non-protective nature of Nb<sub>2</sub>O<sub>5</sub>, the oxidation rate of NbSi<sub>2</sub>, unlike MoSi<sub>2</sub>, is controlled by the interface reaction. The micro-cracks in the arc-melted NbSi<sub>2</sub> increase the exposure area dramatically. On the other hand, the high stress due to volume expansion of oxidation formation at cracks' interior face leads to fragmentation, which in turn results in increased surface

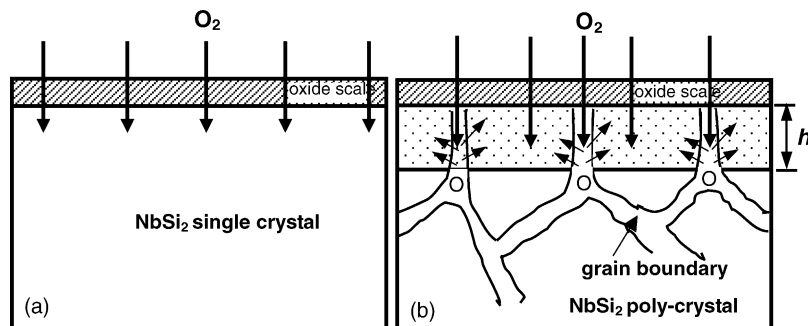


Fig. 5. Schematic drawing showing the oxidation mechanism of ( $h$  is the diffusion depth from the surface to matrix): (a) single crystalline; (b) poly-crystalline MoSi<sub>2</sub>.

area and pesting. Our present work illustrates that accelerated oxidation can be hindered by dense NbSi<sub>2</sub> and single crystal. It was also observed that pesting is hard to happen to dense MoSi<sub>2</sub> poly-crystalline specimen [15], this can be explained in a similar way.

## 5. Conclusions

The oxidation behaviors of single and poly-crystalline NbSi<sub>2</sub> were observed in air at 1023 K. The results show that:

- (1) The pre-existing cracks in the microstructure are main reason to pesting phenomenon. For arc-melted poly-crystalline specimen, NbSi<sub>2</sub> fully turned into powders after 3 h. No pesting was found in the dense SPS poly-crystalline specimens and single crystals after 89 h.
- (2) The oxidation rate is intrinsically determined by the reaction rate between the matrix and the oxygen in air. Nb<sub>2</sub>O<sub>5</sub> scale spalls from the specimen during oxidation. Thus the oxidation kinetics of all the NbSi<sub>2</sub> specimens at 1023 K follows a linear law.
- (3) Grain boundary and pores in the microstructure increase the effective area of oxidation reaction. The oxidation rates of the NbSi<sub>2</sub> samples from high to low are loose poly-crystal, dense poly-crystal and single crystal.

## Acknowledgements

This work was supported by the National Natural Science Foundation of China under a contract #50571067. Provision of high purity raw elements from Kyoto University is also appreciated.

## References

- [1] B.P. Bewlay, J.J. Lewandowski, M.R. Jackson, JOM 40 (8) (1997) 44.
- [2] W.Y. Kim, H. Tanaka, S.J. Hanada, Intermetallics 10 (2002) 625.

- [3] Y. Murayama, S.J. Hanada, Sci. Technol. Adv. Mater. 3 (2002) 145.
- [4] D.M. Shah, D.L. Anton, S. Chin, D.P. Pope, Mater. Sci. Eng. A 192/193 (1995) 658.
- [5] J.J. Rausch, ARF-2981-4, Armour Research Foundation NSA, 1961, 15-31171.
- [6] S.H. Pitman, P. Tsakiroopoulos, in: J. Horton (Ed.), High-Temperature Ordered Intermetallic Alloys VI, J. Mater. Res. Symp. Proc., (364), Material Research Society, Boston, 1995, p. 1321.
- [7] T. Murakami, S. Sasaki, K. Ichikawa, A. Kitahara, Intermetallics 9 (2001) 621.
- [8] T. Murakami, C.N. Xu, M. Kawahara, Y. Takahashi, H. Inui, M. Yamaguchi, Intermetallics 7 (1999) 1043.
- [9] T. Murakami, S. Sasaki, K. Ichikawa, A. Kitahara, Intermetallics 9 (2001) 629.
- [10] J.H. Westbrook, D.L. Wood, J. Nucl. Mater. 12 (1964) 208.
- [11] J. Schlichting, High Temp. High Press. 10 (1978) 241.
- [12] E. Fitzer, W. Remmele, Proceedings of the Fifth International Conference on Composites Materials, AIME, 1985, 515.
- [13] C.G. Mckamey, P.F. Tortorelli, J.H. DeVan, C.A.J. Carmichael, Mater. Res. 7 (1992) 2747.
- [14] D.A. Berztsiss, R.R. Cerchiara, E.A. Cerchiara, F.S. Pettit, G.H. Meier, Mater. Sci. Eng. A 155 (1992) 165.
- [15] K. Kurokawa, H. Houzumi, I. Saeki, H. Takahashi, Mater. Sci. Eng. A 261 (1999) 292.
- [16] T. Maruyama, K. Yanagihara, Mater. Sci. Eng. A 239–240 (1997) 828.
- [17] T.C. Chou, T.G. Nieh, J. Mater. Res. 8 (1) (1993) 214.
- [18] A.D. Shan, F. Wei, H. Hashimoto, Y-H. Park, Scripta Mater. 46 (2002) 645.
- [19] M. Sannia, R.J. Orru, E. Garay, G.Z. Gao, A. Munir, Mater. Sci. Eng. A 345 (2003) 270.
- [20] S. Hiroyuki, Y. Masaru, H. Ken, Y. Osamu, Mater. Res. Bull. 37 (2002) 1557.
- [21] F. Zhang, L.T. Zhang, A.D. Shan, J.S. Wu, Scripta Mater. 53 (2005) 653.
- [22] Z. Song, D.L. Tan, F. He, X.H. Bao, Appl. Surf. Sci. 137 (1999) 142.
- [23] J.W. Zhou, Master Dissertation, Shanghai Jiao Tong University, 2004.
- [24] M.S. Li, High Temperature Corrosion of Metals, Metallurgical Industry Press, Beijing, 2001, p. 36.